Photodiagnosis and Photodynamic Therapy 26 (2019) 342–349

Contents lists available at ScienceDirect

Photodiagnosis and Photodynamic Therapy

journal homepage: www.elsevier.com/locate/pdpdt

Antibacterial photodynamic activity of carbon quantum dots/polydimethylsiloxane nanocomposites against *Staphylococcus aureus, Escherichia coli* and *Klebsiella pneumoniae*

Zoran M. Marković[a,*], Mária Kováčová[b], Petr Humpolíček[c], Milica D. Budimir[a], Jan Vajďák[c], Pavel Kubát[d], Matej Mičušík[b], Helena Švajdlenková[b], Martin Danko[b], Zdenka Capáková[c], Marián Lehocký[c], Biljana M. Todorović Marković[a], Zdeno Špitalský[b,*]

[a] *Vinča Institute of Nuclear Sciences, University of Belgrade, P.O.B. 522, 11001 Belgrade, Serbia*
[b] *Polymer Institute, Slovak Academy of Sciences, Dúbravská cesta 9, 84541 Bratislava, Slovakia*
[c] *Centre of Polymer Systems, Tomas Bata University in Zlín, Trida Tomase Bati 5678, Zlín, Czech Republic*
[d] *J. Heyrovský Institute of Physical Chemistry, Academy of Sciences of the Czech Republic, Dolejškova 3, 182 23 Praha 8, Czech Republic*

ARTICLE INFO

Keywords:
Hydrophobic carbon quantum dots
Medical grade polydimethylsiloxane
Antibacterial surfaces
Visible light sterilization
Antimicrobial photodynamic Therapy

ABSTRACT

Despite great efforts, the design of antibacterial surfaces is still a challenge. In this work, results of structural, mechanical, cytotoxic and antibacterial activities of hydrophobic carbon quantum dots/polydimethylsiloxane surfaces are presented. Antibacterial action of this surface is based on the generation of reactive oxygen species which cause bacteria damage by oxidative stress. At the same time, this surface was not cytotoxic towards the NIH/3T3 cells. Swelling-encapsulation-shrink method is applied for encapsulation of hydrophobic carbon quantum dots in medical grade silicone-polydimethylsiloxane. XPS and photoluminescence spectroscopy analyses confirm that hydrophobic carbon quantum dots have been encapsulated successfully into polydimethylsiloxane polymer matrix. Based on stress-strain test the improvement of mechanical properties of these nanocomposites is established. It is shown by electron paramagnetic resonance spectroscopy and luminescence method that nanocomposite generates singlet oxygen initiated by 470 nm blue light irradiation. Antibacterial testing shows the nanocomposite in the form of foil kills *Staphylococcus aureus, Escherichia coli* and *Klebsiella pneumoniae* and is very effective after only a 15 min irradiation.

1. Introduction

Design of new types of antibacterial surfaces is of great importance due to increased formation of antibiotic-resistant bacteria strains on many surfaces both in healthcare institutions and industries (i.e. food industry or pharmaceutical industry). Formation of these surfaces is a challenge because many parameters such as surface roughness, wettability, surface resistance, surface morphology or surface charge can affect bacteria adhesion and bacteria eradication [1–3]. Apart from surface properties, size and shape as well as charge of bacteria strains play a very significant role in bacteria adhesion to various surfaces [2].

Different strategies have been applied to develop new antibacterial materials. At first, leaching of biocides was used to kill bacteria, i.e. essential oils with biocidal activity were used to develop alternative disinfection strategies for indoor environments or in the food industry, on contaminated surfaces and equipment in food processing environments [4–6]. The drawback of this method is continued development of bacterial resistance. Later, new metal based antibacterial surfaces (coatings of Ag, Cu or Mo) were used to kill bacteria by release of metallic ions [7–9]. Now, apart from surfaces mentioned above, there are new types of antibacterial surfaces or coatings: superhydrophobic ones and those doped by materials that produce reactive oxygen species (singlet oxygen, superoxide, hydroxyl radicals, hydrogen peroxide)-photosensitizers (PS). By applying antibacterial photodynamic therapy (APDT), PS have been excited to a singlet excited state by ultraviolet or visible light. From this state electrons are moving to a triple state or return to a ground state. Singlet oxygen can be generated if they transfer their electrons or energy to molecular oxygen [10,11]. Superhydrophobic surfaces repel bacteria by reducing adhesion forces between bacteria and a surface. In this way, these surfaces enable easy removal of bacteria [12].

Up-to-now many reports referring to antibacterial surfaces which

* Corresponding authors.
E-mail addresses: zoranmarkovic@vin.bg.ac.rs (Z.M. Marković), zdeno.spitalsky@savba.sk (Z. Špitalský).

https://doi.org/10.1016/j.pdpdt.2019.04.019
Received 25 February 2019; Received in revised form 4 April 2019; Accepted 19 April 2019
Available online 22 April 2019

eradicate bacteria by generating reactive oxygen species (ROS) have been published. Polymers (polyurethane, polydimethylsiloxane) doped with different molecules and nanoparticles (porphyrin, methylene blue (MB), crystal violet (CV)/ZnO, Au-MB, carbon quantum dots/Ag) kill wide range of bacteria (*Staphyloccocus aureus (S. aureus), Staphylococcus epidermidis (S. epidermis), Sacchromyces cerevisiae, Escherichia coli* (*E. coli*), *Bacillus subtilis (B. subtilis)*) effectively under visible light [13–20]. Recently, it was shown that graphene nanoplatelets coated on silicone rubber showed strong antibacterial activity toward *S. epidermis* [21].

In this paper we present results of structural, mechanical and antibacterial properties as well as cytotoxicity study of polydimethylsiloxane (PDMS) impregnated by hydrophobic carbon quantum dots (hCQDs). Carbon quantum dots (CQDs) are 0-dimensional nanomaterials with high chemical stability, high photoluminescence, low cost synthesis and resistance to photobleaching [22,23]. As photoactive materials CQDs which are dispersible in water show very good antibacterial and anticancer activity towards different bacteria and cancer cells under blue light irradiation [24–31]. Under ambient light they show very low toxicity against bacteria. Therefore, they can be used for bioimaging [32–35]. To encapsulate CQDs in polymers such as PDMS or polyurethane, they must be dispersible in toluene or acetone which swell used polymer. Because of its biocompatibility, biodurability, antiallergic property, PDMS are widely used in medical devices dominantly as wound care gels, flexible drainage tubes or semi-rigid implants [36]. One of its most important usage is as silicone tubing during hemodialysis [37]. The main request for tubing during hemodialysis is the maintaining of its sterility. Therefore, light irradiated PDMS with encapsulated hCQDs in the form of tube has a very good perspective. In this work we have also investigated how structural and surface properties affected antibacterial activity of hCQDs/ polydimethylsiloxane (hCQDs/PDMS).

2. Experimental

2.1. Preparation of hCQDs and hCQDs/PDMS nanocomposites

The PDMS was prepared by the following: two component polymers were mixed (Silpuran 6000/60 A and Silpuran 6000/60B-Wacker Chemie AG) in ratio 1:1 in a beaker. Hydraulic press (Fontijne Holland SRA 100EC 225 × 320 NA) was heated to 165 °C. Polymer mixture was cured in a mold with thickness of 1 mm between Teflon foils and then compressed with a press of 100 kN for 5 min at 165 °C. Press was cooled down between steel plates for 2 min and dried in oven for 4 h at 200 °C.

The hCQDs were prepared according to procedure described in detail in Ref. [38].

The hCQDs/PDMS nanocomposites were prepared by the following: pieces of PDMS samples (25 × 25 × 1 mm^3) were dipped in hCQDs solution in toluene (50 mL). The concentration of hCQDs was 0.94 mg/mL. Swelling-shrink-encapsulation method was used to encapsulate hCQDs in PDMS. Swelling procedure lasted 28 h at room temperature. The hCQDs nanocomposites were dried at 80 °C for 12 h in vacuum furnace to eliminate toluene from nanocomposites. The scheme for preparation of hCQDs/PDMS nanocomposites is presented in Fig. 1.

2.2. Characterization of hCQDs/PDMS nanocomposites

Swelling measurements of the PDMS and hCQDs/PDMS nanocomposites were conducted at room temperature in toluene. The PDMS and hCQDs/PDMS nanocomposite samples were chopped in 10 × 10 × 1 mm^3 pieces and dipped in solvent for the next 28 h. Samples were weighed every 2 h until constant weight was measured. Measured values from three parallel swelling experiments were averaged. Gravimetric method has been used to calculate the swelling degree [39].

The leaching behaviour of hCQDs/PDMS nanocomposites was determined by the following: samples (10 × 10 × 1 mm^3) were dipped in 20 mL of Milly-Q water for 24 h. UV–vis spectra of water aliquot in which hCQDs/PDMS nanocomposites were immersed, hCQDs/PDMS nanocomposites before and after immersion in water were measured on a Shimadzu UV–vis–NIR SolidSpec-3700 spectrophotometer to check the potential leaching of hCQDs. Leaching experiments were done in triplicate.

The mechanical properties of the prepared samples were characterized by the Instron 3365 (Instron Corporation, USA) at extension of 1 mm/s, which was increased to 5 mm/s after 1% extension of the test sample. For each measurements, 10 samples according norm ASTM D638 were prepared and the results are calculated the arithmetic mean and standard deviation for selected characteristics.

Chemical composition of the hCQDs and hCQDs/PDMS nanocomposites was determined by X-photoelectron spectroscopy (XPS). XPS was performed on Thermo Scientific K-Alpha XPS system using monochromatic Al Kα X-ray source [38]. All XPS measurements were performed three times.

The contact angle (CA) measurements of the PDMS and hCQDs/PDMS nanocomposites were conducted by the Surface Energy Evaluation System (SEE System; Advex Instruments, Czech Republic) and the software from this system has been used for further analysis. Deionized water was used for testing. All tests were repeated three times.

Degradation stability test of neat PDMS and hCQDs/PDMS nanocomposites were conducted under blue light (BL) irradiation for 6 h. Samples were put directly on the lamp at wavelength of 470 nm (3 W, V-TAC, Bulgaria). XPS measurements of both samples were conducted to check the effect of BL on the structure of PDMS and hCQDs/PDMS nanocomposites.

To visualize hCQDs, transmission electron microscopy (TEM-JEOL JEM-1400 operated at 120 kV) was used [38]. The hCQDs were deposited on graphene oxide copper support grid by drop casting and dried at room temperature.

Surface morphology of the PDMS and hCQDs/PDMS nanocomposites was recorded by AFM (Quesant, USA) operated in tapping mode at room temperature. Root-mean-square roughness-RMS of PDMS and hCQDs/PDMS nanocomposites was determined by Gwyddion software [40]. More than 20 AFM images were used for RMS determination.

Photoluminescence (PL) measurements of the hCQDs and hCQDs/PU nanocomposites were performed on a RF-5301PC (Shimadzu, Japan) spectrofluorophotometer at excitation wavelengths between 320 and 480 nm. PL measurements were repeated three times. The homogeneity of the hCQDs/PDMS nanocomposites was verified over the large area PL mapping by confocal Raman microscope (Alpha 300 R, Witec).

Electron paramagnetic spectroscopy (EPR) was used to determine singlet oxygen generation of PDMS and hCQDs/PDMS nanocomposites. 2,2,6,6-tetramethylpiperidine (TEMP) molecules used a spin trap react

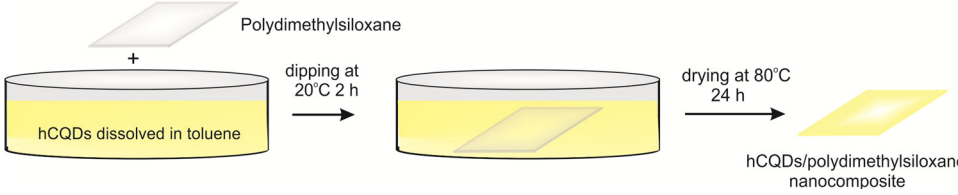

Fig. 1. Schematic view of hCQDs/PDMS nanocomposites preparation.

with $^1O_2$ quickly, and form stable, EPR active product, TEMP-$^1O_2$ (TEMPO). Both samples were dipped in ethanol solutions of 2,2,6,6-tetramethylpiperidine (TEMP). Concentration of TEMP was 2%wt. The EPR experiments were done at room temperature using a Varian E-line spectrometer. The spectrometer operated at a frequency of 9.5 GHz. The hCQDs/PDMS nanocomposites and PDMS control were dipped into TEMP solution. All samples were treated in different conditions: dark, exposed to ambient light (AL) and BL, respectively. The wavelength of BL was 470 nm (3 W, V-TAC, Bulgaria). The EPR spectra of TEMP solutions exposed to BL were measured after 2, 4, 6 and 12 h. EPR experiments were performed in triplicate.

The singlet oxygen formation after excitation of individual samples with Nd:YAG laser (wavelength 355 nm, pulse width ˜5 ns) was measured using time-resolved near-infrared luminescence spectroscopy [41]. Singlet oxygen luminescence at 1270 nm was measured in reflection mode. The measurements were performed in air- and oxygen atmosphere, in vacuum, and with samples immersed in H_2O and D_2O.

2.3. Cytotoxicity determination

Cytotoxicity was determined according to ISO standard 10993-5: cytotoxicity of extracts prepared from the influence of the hCQDs/PU nanocomposites is determined. Sterilization of the samples has been done under the same conditions as for the antibacterial testing. ISO standard 10993-12 was applied to prepare extracts [42]. Mouse embryonic fibroblast cell line (ATCC CRL-1658 NIH/3T3, USA) was used as a model cell line. Cells were seeded at concentration 1×10^5 cell/mL to pre incubate in the micro-titration test plates (TPP, Switzerland) for 24 h. Subsequently, the cultivation media was replaced by previously prepared mixture of culture media with extracts and cultivated for 24 h. Then, MTT assay was used to determine the cell viability [38]. The cytotoxicity is presented as a reduction of cell viability in percentage when compared to cell cultivated in medium without the extracts of tested materials. *t*-test was applied to determine statistical differences.

2.4. Antibacterial testing

The antibacterial testing of the PDMS and hCQDs/PDMS nanocomposites was conducted on *E. coli* CCM 4517, *S. aureus* CCM 4516 and *Klebsiella pneumoniae* (*K. pneumoniae*) CCM 4516. These bacteria strains were purchased from CCM (Czech Collection of Microorganisms). Sterilization by UV lamp (258 nm) of all samples was done for 30 min prior to the testing. Antibacterial activity was conducted according to ISO 22196 standard [38]. Sample dimension was $25 \times 25 \times 1$ mm^3. The concentration of hCQDs inside PDMS for antibacterial measurements was 4.6 mg/cm^3. Used inoculum of *S. aureus* was 1.6×10^6 cfu/mL, *E. coli* was 6.6×10^6 cfu/mL and of *K. pneumoniae* was 1.6×10^6 cfu/mL. To reveal the effect of BL on bacteria strains, PDMS and hCQDs/PDMS nanocomposites were irradiated at 470 nm with power of 15 W for 60 min. The distance from the lamp and samples was 50 cm in order to provide homogeneous illumination of the samples. Equations used for determination of the number of viable bacteria per cm^2 per test specimen and calculation of antibacterial activity are given in Ref. [36]. All testing was done in three experiments, each with four repetitions.

3. Results and discussion

3.1. Swelling degree and leaching behavior of hCQDs/PDMS

Fig. S1a (Supporting information) shows the swelling degree of neat PDMS and hCQDs/PDMS, respectively. Swelling degree was determined for three samples of neat PDMS and hCQDs/PDMS to check the reproducibility of measurement. In Fig. S1a one can notice that there is a time dependence of hCQDs encapsulation inside polymer matrix. The swelling degree of PDMS increases gradually with swelling time. After 4 h of hCQDs encapsulation saturation occurs and further swelling of PDMS contributes to slight hCQDS concentration variation.

Leaching behavior of hCQDs/PDMS nanocomposites is presented in Fig. S1 (b,c). We performed these testing to check whether any leakage of hCQDs from PDMS occurred during time in water environment. Fig. S1b shows absorbance spectra of the hCQDs dissolved in toluene (curve 1) and water aliquot in which hCQDs/PDMS nanocomposites were dipped for 24 h (curve 2). As could be seen from this figure there was not any trace of presence of hCQDs in water after 24 h (Fig. S1b-curve 2). Absorbance spectra of hCQDs/PDMS nanocomposites (curve 1) and hCQDs/PDMS after 24 immersions in water are presented in Fig. S1c. Similar spectra indicate that leakage of hCQDs from polymer does not occur during 24 h. Thus this material can be used in contact with human/animal liquids.

3.2. Stress-strain measurements

Stress-strain measurements have conducted to investigate the effect of hCQDs encapsulation in polymer on mechanical properties of PDMS. PDMS polymer is well-known for its superior properties (chemical stability, high thermal resistance, outstanding insulating properties, low toxicity and low glass temperature) compared to other polymers [43]. This polymer shows low mechanical strength (0.1–0.4 MPa) because Si-O bonds are longer than C—C bonds. Mechanical properties can show stretch ability of polymer before breakage. These properties are very important when polymer is used as antibacterial surface especially its strength, toughness and flexibility. Table S1 shows the Young's modulus, tensile stress and tensile strain at break. Based on data presented in Table S1 Young's modulus has been changed (almost ten times decreased) after hCQDs encapsulation. As for tensile strain and tensile stress values, it is noticed that they increase slightly after hCQDs encapsulation in PDMS. Based on these results we concluded that hCQDs encapsulation in PDMS contributed to variation of Young's modulus of hCQDs/PDMS nanocomposites to a great extent.

3.3. Contact angle measurements

To check surface wettability of neat PDMS and hCQDs/PDMS nanocomposites we conducted CA measurements. Water droplets were deposited on the neat PDMS surface (Fig. S2a) and hCQDs/PDMS nanocomposites (Fig. S2b). Average values of contact angles of neat PDMS and hCQDs/PDMS nanocomposites are $107.8^\circ \pm 2.6^\circ$ and $115.8^\circ \pm 2.6^\circ$, respectively. Encapsulation of hCQDs in polymer matrix affect the surface wettability slightly.

3.4. Chemical analysis

XPS technique was used to determine the content of certain elements presented in PDMS and hCQDs/PDMS as well as structural changes of PDMS polymer after hCQDs encapsulation. Fig. 2 and Tables S2 and S3 show the content of detected elements and characteristic bonds between them in PDMS and hCQDs/PDMS nanocomposites respectively. Based on data presented in Table S2 we noticed that there is an upshift of C1s peak after hCQDs encapsulation (284.26→284.32 eV) and increase of C content for 1.8 At%. As for O and Si contents, encapsulation of hCQDs contributes to decrease of O and Si contents for 0.3 and 1.3 At% respectively. Data listed in Table S3 show that the content of C-Si bonds decreases for 5.4 At% after hCQDs encapsulation whereas the contents of C–O and C═O increase for 0.3 and 0.8 At%. The contents of sp^2 and sp^3 bonds increased after encapsulation of hCQDs for 3.4 and 0.9 At% respectively.

The obtained results of XPS indicate encapsulation of hCQDs in polymer matrix.

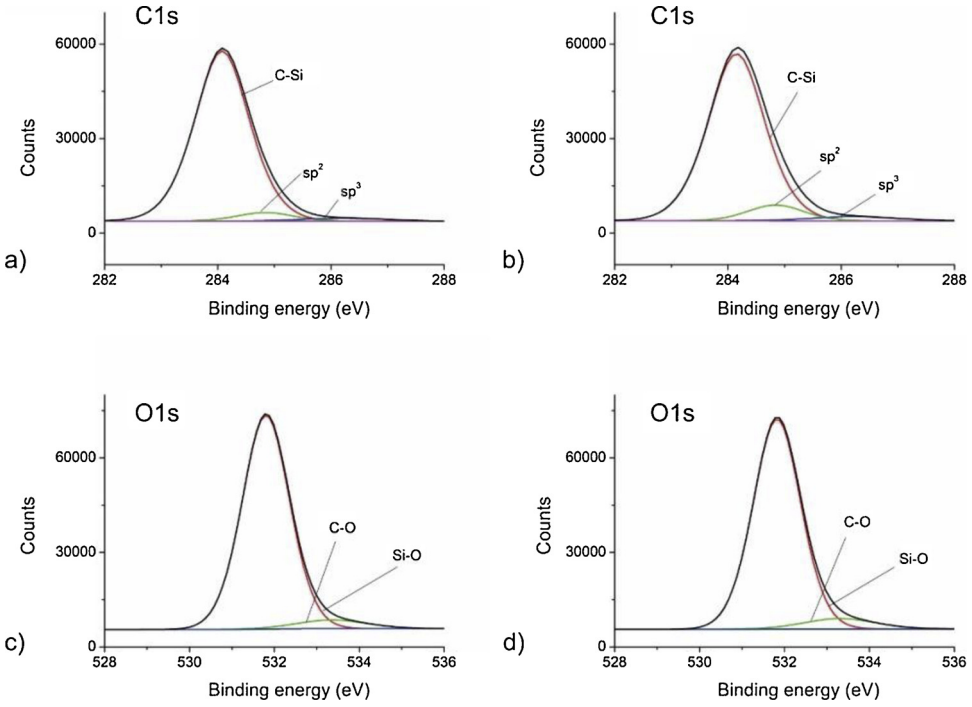

Fig. 2. Deconvoluted XPS spectra of a) C1s peak of PDMS, b) C1s peak of hCQDs/PDMS nanocomposites, c) O1s peak of PDMS and d) O1s peak of hCQDs/PDMS.

3.5. The hCQDs/PDMS nanocomposite degradation

Potential degradation of PDMS polymer and hCQDs/PDMS nanocomposites was investigated by exposing of these samples to BL for 6 h. Results are presented in Tables S2 and S3. XPS results show that BL irradiation of all samples induce minor changes in the contents of C, O and Si. But, after BL irradiation for 6 h, the content of sp^3 increases (3.8 At% for PDMS and 2.5% for hCQDs/PDMS) whereas the content of sp^2 decreases (4.4 At% for PDMS and 4.8% for hCQDs/PDMS). Therefore, BL irradiation contributes to changes in sp^2 and sp^3 both of PDMS and hCQDs/PDMS samples.

3.6. Surface morphology

Fig. 3(a,b) shows top view AFM images of neat PDMS and hCQDs/PDMS nanocomposites as well as TEM micrograph of hCQDs-inset of Fig. 3b. From these figures it could be noticed grain structure of neat PDMS and hCQDs/PDMS nanocomposites. The grain size increases after hCQDs encapsulation in polymer matrix. Surface roughness of neat PDMS is 74.2 nm whereas RMS of hCQDs/PDMS nanocomposites is 86.2 nm. Based on these RMS values we can conclude that hCQDs encapsulation in polymer matrix contributes to increase of surface roughness of nanocomposites. The average size of hCQDs encapsulated in polymer was 5 nm.

3.7. Photoluminescence and PL mapping

Fig. 4(a,b) shows PL intensities of hCQDs and hCQDs/PDMS nanocomposites. As can be seen from Fig. 4b the hCQDs/PDMS nanocomposites emit blue-green light. The highest PL intensity is for 360 nm excitation wavelength whereas the appropriate upshift is 73 cm^{-1}. The highest up-shift (112 cm^{-1}) is for 320 nm excitation wavelength. The blue-green light emission of hCQDs/PDMS nanocomposites is a strong evidence of hCQDs encapsulation inside polymer matrix. Fig. 4c presents optical micrograph of hCQDs/PDMS nanocomposites including overlay of PL mapping. This figure shows homogenous PL across the whole nanocomposites without any streaks which is a clear evidence of hCQDs encapsulation inside PDMS.

In our previous research we established that PL property of hCQDs occurs due to the confinement effects and recombination of electron–hole pairs. Recombination of electron-hole pairs occurs dominantly in small sp^2 islands surrounding by sp^3 carbon network. The other important factor that contributes to PL of hCQDs is surface defects caused by the presence of oxygen functional groups over the surface and edges

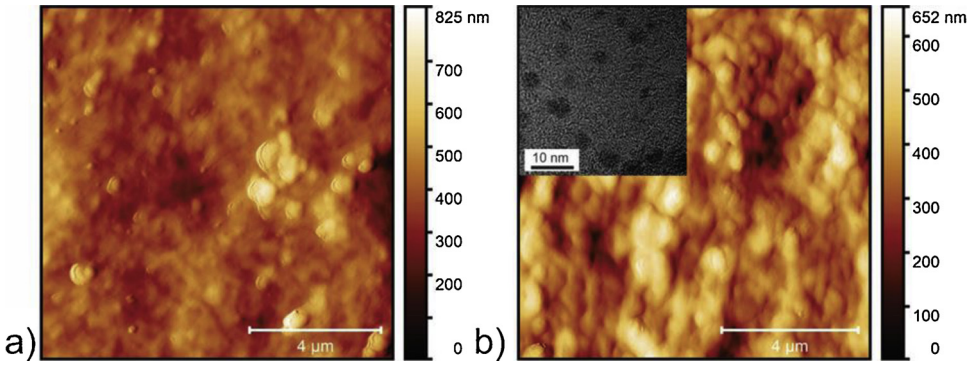

Fig. 3. Top view AFM images of pure PDMS (a) and hCQDs/PDMS nanocomposites (b); TEM micrograph of hCQDs-inset of Fig. 1b.

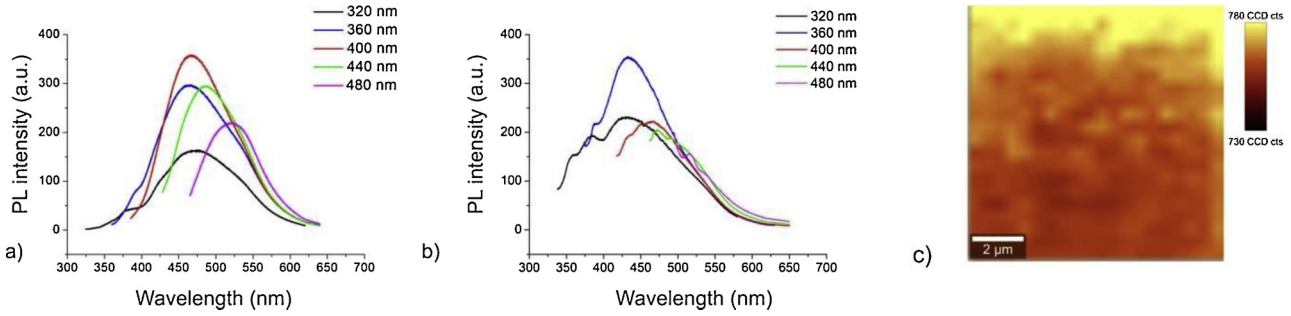

Fig. 4. PL spectra of a) hCQDs and b) PL of hCQDs/PDMS nanocomposites; c) optical micrograph of hCQDs/PDMS nanocomposites including overlay of PL mapping.

of the hCQDs [44,45]. Since hCQDs/PDMS nanocomposites emit blue-green light under different excitation wavelengths we concluded that hCQDs encapsulated inside polymer retain their PL property.

3.8. Singlet oxygen generation detemined by EPR and luminescence measurements

EPR and luminescence measurements have been performed to measure singlet oxygen production of hCQDs/PDMS nanocomposites. Singlet oxygen belongs to a group of ROS which are responsible for death of different bacteria strains and cancer cells. It is a very reactive form of oxygen that effectively destroy bacteria membrane wall, kill malignant cells by apoptosis and/or necrosis, shut down the tumor microvasculature and stimulate the host immune system [46]. To follow the formation of singlet oxygen ($^1O_2$), 2,2,6,6-tetramethylpiperidine (TEMP) was used as a spin trap. At the beginning we tested neat PDMS polymer for singlet oxygen production. We established that this sample does not produce singlet oxygen under any conditions.

Fig. 5a,b presents singlet oxygen generation by hCQDs/PDMS nanocomposites under different conditions: in dark, AL for 12 h and BL with different irradiation time (2, 4, 6 and 12 h). As can be noticed from Fig. 5a, hCQDs/PDMS nanocomposites did not produce singlet oxygen in dark and under AL irradiation for 12 h. But during irradiation by BL hCQDs/PDMS nanocomposites start to generate singlet oxygen already after 6 h of irradiation. Massive production of singlet oxygen occurs after 12 h of BL.

Apart from EPR spectroscopy where EPR signals reflect only singlet oxygen diffused to nanocomposite environment and formed a complex with TEMP, we used luminescence at 1270 nm method to determine singlet oxygen production of hCQDs in polymer matrix and its decay in both polymer matrix and its environment (Fig. 5c). The calculated lifetime of singlet oxygen photogenerated by the hCQDs/PDMS nanocomposite is 45 μs-(Fig. S3a), which is relatively high value in comparison with other polymeric matrices [47]. Fig. 5c shows laser excited singlet oxygen luminescence of the hCQDs/PDMS nanocomposites as a function of time - data are corrected to signals in vacuum, where no singlet oxygen is formed. From this figure it is obvious that hCQDs/PDMS nanocomposites produce singlet oxygen. In this way polymer serves as a reservoir of singlet oxygen with relatively high lifetime. Removal of oxygen from PDMS needs at least 30 min of evacuation by rotatory pump.

Longer rise time indicates presence of relatively long lived excited states that is quenched by oxygen to form singlet oxygen. Immersion of hCQDs/PDMS into H_2O (with lifetime of singlet oxygen about 3.5 μs) slightly influenced calculated singlet oxygen lifetime (from 45 ± 1 to 42 ± 2 μs in H_2O) (Fig. S3b). These observations indicate that luminescence of singlet oxygen comes predominantly from the bulk of polymer with minor contribution of singlet oxygen diffused to H_2O. In contrast to previous study of hCQDs/polyurethane nanocomposites with lower lifetime of singlet oxygen (˜12 μs) [48], hCQDs/PDMS nanocomposites serve as a reservoir of singlet oxygen for relatively high time after excitation (several tens of μs) and can gradually release singlet oxygen to their environment, where is effectively quenched. The small amount of singlet oxygen diffused outside polymer is probably due low surface-to-volume ratio of samples. Nanoparticles or nanofiber materials with high surface-to-volume ratio should better release singlet oxygen to the environment for photo-oxidation of biological structures. The diffusion path of singlet oxygen in H_2O is tens to hundreds of nm during its lifetime [41]. This means that bacteria (or other biological/chemical species) should be in close contact with surfaces for efficient antibacterial activity.

Possible mechanisms of single oxygen generation by CQDs were described in the literature: a) singlet oxygen is generated through energy transfer to molecular oxygen [49], b) there is an additional step in singlet oxygen generation (generation of superoxide anion). In this way, electron transfer is an intermediate step for singlet oxygen generation by GQDs [50]. Based on results presented above and our previous results [29] we concluded that energy transfer has dominant role in singlet oxygen production of hCQDs/PDMS nanocomposites.

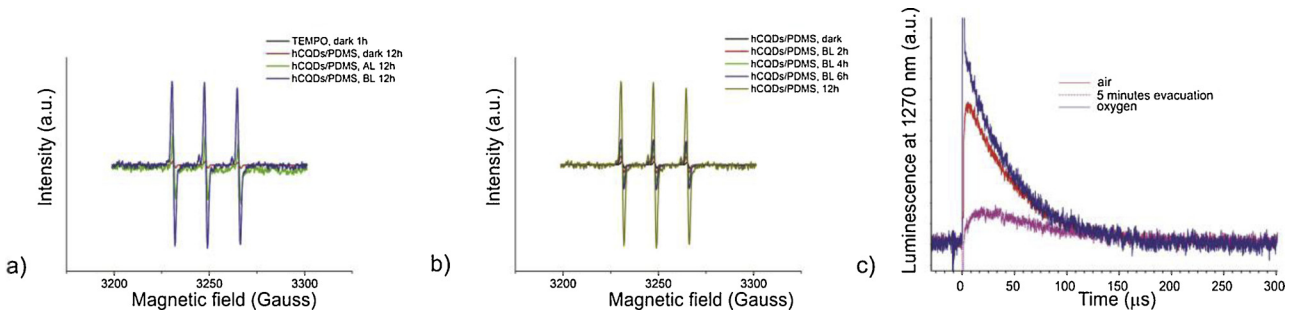

Fig. 5. a) EPR spectra of the TEMPO sample (black curve), and the hCQDs/PDMS nanocomposites in dark (red curve), under AL (green curve), under BL (blue curve) for 12 h; b) EPR spectra of hCQDs/PDMS nanocomposites under different BL irradiation time; c) Laser excited singlet oxygen luminescence of the hCQDs/PDMS nanocomposites vs. time - data are corrected to signals in vacuum, where no singlet oxygen is formed.

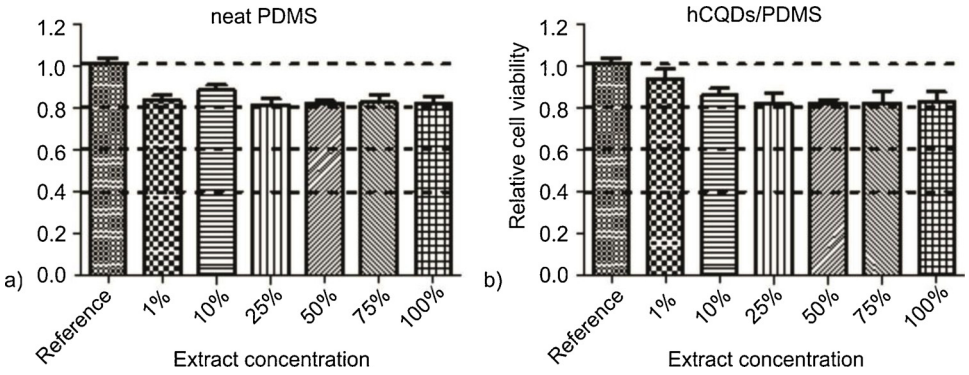

Fig. 6. NIH/3T3 cell viability in various extract concentrations. Cytotoxicity in relative values equal to 1 corresponds to 100% cell survival compared to reference. Values > 0.8 are assigned to no cytotoxicity, 0.6–0.8 to mild cytotoxicity, 0.4–0.6 to moderate cytotoxicity, and < 0.4 to severe cytotoxicity.

3.9. Cytotoxicity of hCQDs/PDMS nanocomposites

It is very important to investigate cytotoxic property of hCQDs/PDMS nanocomposites due to their possible usage as antibacterial surface. Cytotoxicity of hCQDs/PDMS nanocomposites was determined by MTT assay. The methodology of testing is in accordance to the ISO standard, where the cells are cultivated in presence of either pure cultivation medium or cultivation medium mixed with various concentration of extract from tested samples. The NIH/3T3 cell line was used as standard cell line for cytotoxicity testing. In Fig. 6 results of cell viability in various extract concentrations are presented. We tested neat PDMS and hCQDs/PDMS nanocomposites.

As could be seen from Fig. 6a neat PDMS is not cytotoxic no matter extract concentration whereas hCQDs/PDMS nanocomposites do not show any cytotoxicity as well. Results induce possible usage of hCQDs/PDMS nanocomposites as a medical device for short term contact with human body.

3.10. Antibacterial assay

To investigate antibacterial activity of hCQDs/PDMS nanocomposites towards Gram positive and Gram negative bacteria strains we conducted antibacterial testing against three bacteria: *S. aureus, E.coli* and *K. pneumoniae*. Results are presented in Table 1.

Based on results presented in Table 1 we noticed that neat PDMS did not show any antibacterial activity with or without BL. Samples were irradiated by BL at 470 nm because it had earlier reported that light with wavelength longer than 405 nm did not eradicate bacteria itself [51].

As for hCQDs/PDMS nanocomposites they showed very good activity towards *S. aureus, E. coli* and *K. pneumoniae*. Namely, after 15 min irradiation by BL, *S. aureus, E. coli* and *K.pneumoniae* were eradicated completely. Therefore, *S. aureus, E. coli* and *K. pneumoniae* are very sensitive to hCQDs/PDMS samples irradiated by BL. The possible mechanism for bacterial death can be the following: ROS (generated singlet oxygen in our case) damage bacterial cell wall and cause bacterial death by oxidative stress. The generation and clearance of ROS in bacterial cells are balanced in normal conditions. But when the excessive production of ROS is presented (under the effect of hCQDs) the redox balance of cell favors oxidation. This unbalanced state produces oxidative stress, which damages the individual components of bacterial cells [52].

Antibacterial results presented above are very important because *S. aureus* is transmitted through contact with the organism in a purulent lesion or on the hands. Furthermore, burn units are contaminated very easily. This bacteria can remain virulent for 10 days on dry surfaces. *K. pneumoniae* is transmitted through contact with contaminated surfaces and objects, medical equipment and blood products and can remain more than 2 h on dry inanimate surfaces [53]. The usage of hCQDs/PDMS nanocomposites under BL as antibacterial surfaces can contribute dramatically to efficient eradication of these bacteria strains because they are killed only after 15 min of BL irradiation. Compared to our previous results related to hCQDs/polyurethane (hCQDs/PU) nanocomposites, the hCQDs/PDMS showed better antibacterial effects towards *S. aureus* and *E. coli* [48]. The hCQDs/PDMS nanocomposites showed better antibacterial results compared to CV-MgO/PU, CV-ZnO/PU nanocomposites as well as Cu/PU and MB-Au/PDMS nanocomposites [17,54,55].

3.11. The effect of surface roughness and wettability on antibacterial activity

Different properties of materials need to be considered (surface energy, wettability, surface charges, surface roughness) to design antibacterial surfaces which kill various bacteria strains effectively. There are many studies reported the effect of surface wettability on bacteria adhesion [3]. Surfaces with moderate wettability are more favorable compared to high hydrophobic or hydrophilic surface. Materials with low surface energy adhere weaker bacteria than materials with higher surface energy. Surface roughness is very important parameter of each surface but the effect of this parameter is limited because the shape and size of bacteria can also play very significant role in bacterial interaction with surfaces. In this section we have compared RMS, CA and antibacterial activity for three materials with hCQDs: Langmuir-

Table 1
Antibacterial activity of neat PDMS and hCQDs/PDMS nanocomposites towards *S. aureus, E. coli* and *K. pneumoniae.* Nanocomposites were irradiated by BL for 15 min and 60 min.

Samples	Time (min)	*S. aureus*		*E. coli*		*K.pneumoniae*	
		N (cfu/cm^2)	R = U_t-A_t	N (cfu/cm^2)	R = U_t-A_t	N (cfu/cm^2)	R = U_t-A_t
PDMS	15	1.7×10^7	U_t=5.1	4.3×10^6	U_t=5.5	2.3×10^6	U_t = 5.2
hCQDs/PDMS	15	< 1	≥5.1	< 1	≥5.5	< 1	≥5.2
PDMS	60	1.1×10^5	U_t = 5.04	7.6×10^5	U_t=5.8	1.1×10^5	U_t = 5.04
hCQDs/PDMS	60	< 1	≥5.04	< 1	≥5.8	< 1	≥5.04

Table 2
RMS, contact angles (CA) and antibacterial efficiency of three different systems: LBhCQDs/SiO_2, hCQDs/PU and hCQDs/PDMS.

Samples	RMS (nm)	CA (°)	Antibacterial efficiency
LBhCQDs/SiO_2	0.3	99.9	moderate
hCQDs/PU	3.05	111.9	excellent
hCQDs/PDMS	86.2	107.8	excellent

Blodgett (LB) hCQDs thin films [38], hCQDs/PU [48] and hCQDs/PDMS nanocomposites. Table 2 presents results of RMS, CA and antibacterial activity of LB hCQDs thin films deposited on SiO_2 (LBhCQDs/SiO_2) [38], hCQDs/PU nanocomposites [48] and hCQDs/PDMS nanocomposites.

As can be seen from Table 2 variation of CA values are not so significant. On the other hand, range of RMS values is quite large. Katsikogianni and Missirlis showed that bacteria dominantly adhere to surface topography features as large as their own diameters [56,57]. They claimed also that asperity size as well as its shapes affect strongly bacterial adhesion. In our investigation, we established that rougher polymer surface has bigger diffusion channels of singlet oxygen than smoother surfaces. Faster diffusion of singlet oxygen to surface decreases time of eradication of the investigated bacteria.

All three sample types did not show any antibacterial activity without BL irradiation. Under BL irradiation all sample show moderate to excellent antibacterial activity. Furthermore, the hCQDs/PDMS nanocomposites are bactericidal not only towards *S. aureus* and *E. coli* but against *K. pneumoniae*. The latter bacteria is common for any type of healthcare facilities and formation of antibacterial surfaces with high efficacy was a big challenge.

In our research we supposed that generation of singlet oxygen by hCQDs had a key role in antibacterial activity of hCQDs/PDMS nanocomposites. But, surface roughness of hCQDs/PDMS nanocomposites contributed significantly to better adhesion of bacteria to surface and their further effective elimination.

4. Conclusions

In this paper we have investigated structural, mechanical properties and antibacterial activity of hCQDs/PDMS nanocomposites. The hCQDs has been encapsulated in polymer by simple swelling-encapsulation-shrink method. Different characterization techniques have shown that hCQDs were encapsulated in PDMS successfully, they retained their PL and ability of singlet oxygen production. Young's moduls of hCQDs/PDMS nanocomposites has been changed to a great extent where tensile strength and tensile stress has been varied slightly. BL irradiated polymer serves as a reservoir of singlet oxygen with relatively high lifetime. Large surface roughness of 86.2 nm significantly promoted fast singlet oxygen diffusion to the surface.

Low power BL source triggered singlet oxygen generation in the hCQDs/PDMS nanocomposites. In this way nanocomposite eradicated 5logs of *S. aureus*, *E. coli* and *K. Pneumoniae* in 15 min. On the other side, this nanocomposite is not cytotoxic towards the NIH/3T3 cells. In this way, the hCQDs/PDMS nanocomposite is a promising candidate for visible light triggered sterilization application in hospitals, pharmaceutical or food industries.

Acknowledgements

Author Zoran Marković thanks for support to SASPRO Programme project1237/02/02-b as well as the People Programme (Marie Curie Actions) European Union's Seventh Framework Programme under REA grant agreement No. 609427. Authors Zdeno Špitalský and Maria Kováčová acknowledge support of the VEGA (2/0093/16). Authors Petr Humpolíček, Zdenka Capáková, Jan Vajďák and Marián Lehocký thank the Ministry of Education, Youth and Sports of the Czech Republic - Program NPU I (LO1504). Author Pavel Kubát thanks for support to Czech Science Foundation (No. 19-09721S). Authors Biljana Todorović Marković, Zoran Marković and Milica Budimir thank for support to the Ministry of Education, Science and Technological Development of the Republic of Serbia via project no. 172003, bilateral project Serbia-SlovakiaSK-SRB-2016-0038, and multilateral scientific and technological cooperation in the Danube region (DS-2016-021).

Appendix A. Supplementary data

Supplementary material related to this article can be found, in the online version, at doi:https://doi.org/10.1016/j.pdpdt.2019.04.019.

References

[1] X. Zhang, L. Wang, E. Levanen, Superhydrophobic surfaces for the reduction of bacterial adhesion, RSC Adv. 3 (2013) 12003, https://doi.org/10.1039/C3RA40497H.
[2] J.A. Lichter, K.J. Van Vliet, M.F. Rubner, Design of antibacterial surfaces and interfaces: polyelectrolyte multilayers as a multifunctional platform, Macromolecules 42 (2009) 8573–8586, https://doi.org/10.1021/ma901356s.
[3] Y. Yuan, M.P. Hays, P.R. Hardwidge, J. Kim, Surface characteristics influencing bacterial adhesion to polymeric substrates, RSC Adv. 7 (2017) 14254, https://doi.org/10.1039/C7RA01571B.
[4] A. Puškárová, M. Bučková, L. Kraková, D. Pangallo, K. Kozics, The antibacterial and antifungal activity of six essential oils and their cyto/genotoxicity to human HEL 12469 cell, Sci. Rep. (2017) 8211, https://doi.org/10.1038/s41598-017-08673-9.
[5] K. Lépesová, L. Kraková, D. Pangallo, A. Medveďová, P. Olejníková, T. Mackuľak, J. Tichý, R. Grabic, L. Birošová, Prevalence of antibiotic resistant coliform bacteria, Enterococcus spp. and Staphylococcus spp. in wastewater sewerage biofilm, J. Glob. Antimicrob. Resist. 14 (2018) 145–151, https://doi.org/10.1016/j.jgar.2018.03.008.
[6] M. Bučková, A. Puškárová, V. Kalászová, Z. Kisová, D. Pangallo, Essential oils against multidrug resistant gram-negative bacteria, Biologia 73 (2018) 803–808, https://doi.org/10.2478/s11756-018-0090-x.
[7] M. Rai, A. Yadav, A. Gade, Silver nanoparticles as a new generation of antimicrobials, Biotechnol. Adv. 27 (2009) 76–83, https://doi.org/10.1016/j.biotechadv.2008.09.002.
[8] M.T. Hsiao, S.F. Chen, D.B. Shieh, C.S. Yeh, One-pot synthesis of hollow Au_3Cu_1 spherical-like and biomineral botallackite $Cu_2(OH)_3Cl$ flowerlike architectures exhibiting antimicrobial activity, J. Phys. Chem. B 110 (2006) 205–210, https://doi.org/10.1021/jp054827x.
[9] M. Yasuyuki, K. Kunihiro, S. Kurissery, N. Kanavillil, Y. Sato, Y. Kikuchi, Antibacterial properties of nine pure metals: a laboratory study using *Staphylococcus aureus* and Escherichia coli, Biofouling 26 (2010) 851–858, https://doi.org/10.1080/08927014.2010.527000.
[10] T. Dai, Y. Huang, M.R. Hamblin, Photodynamic therapy for localized infections–State of the art, Photodiagn. Photodyn. Ther. 6 (2009) 170–188, https://doi.org/10.1016/j.pdpdt.2009.10.008.
[11] T. Maisch, J. Baier, B. Franz, M. Maier, M. Landthaler, R. Szeimies, W. Bäumler, The role of singlet oxygen and oxygen concentration in photodynamic inactivation of bacteria, Proc. Natl. Acad. Sci. U. S. A. 104 (2007) 7223–7228, https://doi.org/10.1073/pnas.0611328104.
[12] C.R. Crick, S. Ismail, J. Pratten, I.P. Parkin, An investigation into bacterial attachment to an elastomeric superhydrophobic surface prepared via aerosol assisted deposition, Thin Solid Films 519 (2011) 3722–3727, https://doi.org/10.1016/j.tsf.2011.01.282.
[13] A. Felgenträger, T. Maisch, A. Spath, J.A. Schroder, W. Baumler, Singlet oxygen generation in porphyrin-doped polymeric surface coating enables antimicrobial effects on Staphylococcus aureus, Phys. Chem. Chem. Phys. 16 (2014) 20598, https://doi.org/10.1039/c4cp02439g.
[14] T. Walker, M. Canales, S. Noimark, K. Page, I. Parkin, J. Faull, M. Bhatti, L. Ciric, A light activated antimicrobial surface is active against bacterial, viral and fungal organisms, Sci. Rep. 7 (2017) 15298, https://doi.org/10.1038/s41598-017-15565-5.
[15] S. Perni, C. Piccirillo, J. Pratten, P. Prokopovich, W. Chrzanowski, I.P. Parkin, M. Wilson, The antimicrobial properties of light-activated polymers containing methylene blue and gold nanoparticles, Biomaterials 30 (2009) 89–93, https://doi.org/10.1016/j.biomaterials.2008.09.020.
[16] C. Piccirillo, S. Perni, J. Gil-Thomas, P. Prokopovich, M. Wilson, J. Pratten, I.P. Parkin, Antimicrobial activity of methylene blue and toluidine blue o covalently bound to a modified silicone polymer surface, J. Mater. Chem. 19 (2009) 6167–6171, https://doi.org/10.1039/B905495B.
[17] S.K. Sehmi, S. Noimark, S.D. Pike, J.C. Bear, W.J. Peveler, C.K. Williams, M.S.P. Shaffer, E. Allan, I.P. Parkin, A.J. MacRobert, Enhancing the antibacterial activity of light-activated surfaces containing crystal violet and ZnO nanoparticles: investigation of nanoparticle size, capping ligand, and dopants, ACS Omega 1 (2016) 334–343, https://doi.org/10.1021/acsomega.6b00017.
[18] A.J.T. Naik, S. Ismail, C. Kay, M. Wilson, I.P. Parkin, Antimicrobial activity of polyurethane embedded with methylene blue, toluidene blue and gold

nanoparticles against *Staphylococcus aureus* illuminated with white light, Mater. Chem. Phys. 129 (2011) 446–450, https://doi.org/10.1016/j.matchemphys.2011.04.040.
[19] C. Xing, Q. Xu, H. Tang, L. Liu, S. Wang, Conjugated polymer/porphyrin complexes for efficient energy transfer and improving light-activated antibacterial activity, J. Am. Chem. Soc. 131 (2009) 13117–13124, https://doi.org/10.1021/ja904492x.
[20] R. Duarah, Y.P. Singh, P. Gupta, B.M. Mandal, N. Karak, High performance bio-based hyperbranched polyurethane/carbon dot-silver nanocomposite: a rapid self-expandable stent, Biofabrication 8 (2016) 045013, , https://doi.org/10.1088/1758-5090.
[21] R.N. Gomes, I. Borges, A.T. Pereira, A.F. Maia, M. Pestana, F.D. Magalhaes, A.M. Pinto, I.C. Gonçalves, Antimicrobial graphene nanoplatelets coatings for silicone catheters, Carbon 139 (2018) 635e647, , https://doi.org/10.1016/j.carbon.2018.06.044.
[22] R. Jelinek, Carbon Quantum Dots: Synthesis, Properties, Applications, Springer International Publishing, 978-3-319-43911-2, 2017.
[23] S.P. Jovanović, Z. Syrgiannis, Z.M. Marković, A. Bonasera, D.P. Kepić, M. Budimir, D.D. Milivojević, V.D. Spasojević, M.D. Dramićanin, V.B. Pavlović, B.M. Todorović Marković, Modification of structural and luminescence properties of graphene quantum dots by gamma irradiation and their application in a photodynamic therapy, ACS Appl. Mater. Inter. 7 (2015) 25865–25874, https://doi.org/10.1021/acsami.5b08226.
[24] N.A. Travlou, D.A. Giannakoudakis, M. Algarra, A.M. Labella, E. Rodríguez-Castellón, T.J. Bandosz, S- and N-doped carbon quantum dots: surface chemistry dependent antibacterial activity, Carbon 135 (2018) 104–111, https://doi.org/10.1016/j.carbon.2018.04.018.
[25] X. Dong, M. Al Awak, N. Tomlinson, Y. Tang, Y.P. Sun, L. Yang, Antibacterial effects of carbon dots in combination with other antimicrobial reagents, PLoS One 12 (2017) e0185324, , https://doi.org/10.1371/journal.pone.0185324.
[26] H. Li, J. Huang, Y. Song, M. Zhang, H. Wang, F. Lu, H. Huang, Y. Liu, X. Dai, Z. Gu, Z. Yang, R. Zhou, Z. Kang, Degradable carbon dots with broad-spectrum antibacterial activity, ACS Appl. Mater. Interfaces 10 (2018) 26936–26946, https://doi.org/10.1021/acsami.8b08832.
[27] M.M. Al Awak, P. Wang, S. Wang, Y. Tang, Y.P. Sun, L. Yang, Correlation of carbon dots' light-activated antimicrobial activities and fluorescence quantum yield, RSC Adv. 7 (2017) 30177–30184, https://doi.org/10.1039/C7RA05397E.
[28] A. Kumer Roy, S.M. Kim, P. Paoprasert, S.Y. Park, I. In, Preparation of biocompatible and antibacterial carbon quantum dots derived from resorcinol and formaldehyde spheres, RSC Adv. 5 (2015) 31677–31682, https://doi.org/10.1039/C5RA01506E.
[29] Z.M. Marković, S.P. Jovanović, P.Z. Mašković, M. Danko, M. Mičušik, V.B. Pavlović, D.D. Milivojević, A. Kleinova, Z. Špitalsky, B.M. Todorović Marković, Photo-induced antibacterial activity of four graphene based nanomaterials on a wide range of bacteria, RSC Adv. 8 (2018) 31337, https://doi.org/10.1039/C8RA04664F.
[30] Z.M. Marković, B.Z. Ristić, K.M. Arsikin, Dj.G. Klisić, Lj.M. Harhaji-Trajković, B.M. Todorović-Marković, D.P. Kepić, T.K. Kravić-Stevović, S.P. Jovanović, M.M. Milenković, D.D. Milivojević, V.Z. Bumbasirević, M.D. Dramićanin, V.S. Trajković, Graphene quantum dots as autophagy-inducing photodynamic agents, Biomaterials 33 (2012) 7084–7092, https://doi.org/10.1016/j.biomaterials.2012.06.060.
[31] J. Pardo, Z. Peng, R.M. Leblanc, Cancer targeting and drug delivery using carbon-based quantum dots and nanotubes, Molecules 10 (2018) 23, https://doi.org/10.3390/molecules23020378.
[32] H. Liu, Z. Li, Y. Sun, X. Geng, Y. Hu, H. Meng, J. Ge, L. Qu, Synthesis of luminescent carbon dots with ultrahigh quantum yield and inherent folate receptor-positive cancer cell targetability, Sci. Rep. 8 (2018) 1086, https://doi.org/10.1038/s41598-018-19373-3.
[33] C.F. Li, Z.K.M. Yan, L.B. Chen, J.P. Jin, D.D. Li, Desmin detection by facile prepared carbon quantum dots for early screening of colorectal cancer, Medicine 96 (2017) e5521, https://doi.org/10.1097/MD.0000000000005521.
[34] P.G. Luo, S. Sahu, S.T. Yang, S.K. Sonkar, J. Wang, H. Wang, G.E. LeCroy, L. Cao, Y.P. Sun, Carbon "quantum" dots for optical bioimaging, J. Mater. Chem. B 1 (2013) 2116.
[35] K. Hola, Y. Zhang, Y. Wang, E.P. Giannelis, R. Zboril, A.L. Rogach, Carbon dots—emerging light emitters for bioimaging, cancer therapy and optoelectronics, Nanotoday 9 (2014) 590–603, https://doi.org/10.1039/C3TB00018D.
[36] http://www.fostercomp.com/silicones-medical-devices.
[37] K. Marion-Ferey, M. Pasmore, P. Stoodley, S. Wilson, G.P. Husson, J.W. Costerton, Biofilm removal from silicone tubing: an assessment of the efficacy of dialysis machine decontamination procedures using an in vitro model, J. Hosp. Infect. 53 (2003) 64–71, https://doi.org/10.1053/jhin.2002.1320.
[38] N.K. Stanković, M. Bodik, P. Siffalovic, M. Kotlar, M. Mičušik, Z. Špitalsky, M. Danko, D.D. Milivojević, A. Kleinova, P. Kubat, Z. Capakova, P. Humpoliček, M. Lehocky, B.M. Todorović Marković, Z.M. Marković, Antibacterial and anti-biofouling properties of light triggered fluorescent hydrophobic carbon quantum dots Langmuir – Blodgett thin films, ACS Sustain. Chem. Eng. 6 (2018) 4154–4163, https://doi.org/10.1021/acssuschemeng.7b04566.
[39] J.V. Džunuzović, M.V. Pergal, S. Jovanović, V.V. Vodnik, Synthesis and swelling behavior of polyurethane networks based on hyperbranched polymer, Hem. Ind. 65 (2011) 637–644, https://doi.org/10.2298/HEMIND110902071D.
[40] D. Nečas, P. Klapetek, Gwyddion: open-source software for SPM data analysis, Cent. Eur. J. Phys. 10 (2012) 181–188, https://doi.org/10.2478/s11534-011-0096-2.
[41] P. Henke, K. Kirakci, P. Kubát, M. Fraiberk, J. Forstová, J. Mosinger, Polystyrene nanofiber materials modified with an externally bound porphyrin photosensitizer, ACS Appl. Mater. Interfaces 8 (2016) 25127, https://doi.org/10.1021/am4004057.
[42] L. Musilova, A. Mráček, A. Kovalčik, P. Smolka, A. Minarik, P. Humpoliček, R. Vicha, P. Ponižil, Hyaluronan hydrogels modified by grlycinated kraft lignin: morphology, swelling, viscoelastic properties and biocompability, Carbohydr. Polym. 181 (2018) 394–403, https://doi.org/10.1016/j.carbpol.2017.10.048.
[43] N.J. Huang, J. Zang, G.D. Zhang, L.Z. Guan, S.N. Li, L. Zhao, L.C. Tang, Efficient interfacial interaction for improving mechanical properties of polydimethylsiloxane nanocomposites filled with low content of graphene oxide nanoribbons, RSC Adv. 7 (2017) 22045, https://doi.org/10.1039/C7RA02439H.
[44] H. Yan, C. He, X. Li, T. Zhao, A solvent-free gaseous detonation approach for converting benzoic acid into graphene quantum dots within milliseconds, Diam. Relat. Mater. 87 (2018) 233–241, https://doi.org/10.1016/j.diamond.2018.06.008.
[45] S.P. Jovanović, Z.M. Marković, Z. Syrgiannis, M. Dramićanin, F. Arcudi, V. La Parola, M. Budimir, B.M. Todorović Marković, Enhancing photoluminescence of graphene quantum dots by thermal annealing of the graphite precursor, Mater. Res. Bull. 93 (2017) 183–193, https://doi.org/10.1016/j.materresbull.2017.04.052.
[46] B. Li, L. Lin, H. Lin, B.C. Wilson, Photosensitized singlet oxygen generation and detection: recent advances and future perspectives in cancer photodynamic therapy, J. Biophotonics 9 (2016) 1314–1325, https://doi.org/10.1002/jbio.201600055.
[47] K. Schiller, F.W. Miller, Singlet oxygen lifetime in polymer films, Polym. Int. 25 (1991) 19–22, https://doi.org/10.1002/pi.4990250105.
[48] M. Kováčová, Z.M. Marković, P. Humpolíček, M. Mičušík, H. Švajdlenková, A. Kleinová, M. Danko, P. Kubát, J. Vajďák, Z. Capáková, M. Lehocký, L. Münster, B.M. Todorović Marković, Z. Špitalský, Carbon quantum dots modified polyurethane nanocomposites as effective photocatalytic and antibacterial agents, ACS Biomater. Sci. Eng. 4 (2018) 3983–3993, https://doi.org/10.1021/acsbiomaterials.8b00582.
[49] J. Ge, M. Lan, B. Zhou, W. Liu, L. Guo, H. Wang, Q. Jia, G. Niu, X. Huang, H. Zhou, X. Meng, P. Wang, C.S. Lee, W. Zhang, X.A. Han, Graphene quantum dot photodynamic therapy agent with high singlet oxygen generation, Nat. Commun. 5 (2014) 4596, https://doi.org/10.1038/ncomms5596.
[50] Y. Chong, C. Ge, G. Fang, X. Tian, X. Ma, T. Wen, W.G. Wamer, C. Chen, Z. Chai, J.J. Yin, Crossover between anti- and pro-oxidant activities of graphene quantum dots in the absence or presence of light, ACS Nano 10 (2016) 8690, https://doi.org/10.1021/acsnano.6b04061.
[51] M.D. Barneck, N.L.R. Rhodes, M. De la Presa, J.P. Allen, A.E. Poursaid, M.M. Nourian, M.A. Firpo, J.T. Langell, Violet 405-nm light: a novel therapeutic agent against common pathogenic bacteria, J. Surg. Res. 206 (2016) 316–324, https://doi.org/10.1016/j.jss.2016.08.006.
[52] L. Wang, C. Hu, L. Shao, The antimicrobial activity of nanoparticles: present situation and prospects for the future, Int. J. Nanomed. 12 (2017) 1227–1249, https://doi.org/10.2147/IJN.S121956.
[53] W. Lou, S. Venkataraman, G. Zhong, B. Ding, J.P.K. Tan, L. Xu, W. Fan, Y.Y. Yang, Antimicrobial polymers as therapeutics for treatment of multidrug-resistant *Klebsiella pneumoniae* lung infection, Acta Biomater 15 (2018) 78–88, https://doi.org/10.1016/j.actbio.2018.07.038.
[54] S.K. Sehmi, S. Noimark, J. Weiner, E. Allan, A.J. MacRobert, I.P. Parkin, Potent antibacterial activity of copper embedded into silicone and polyurethane, ACS Appl. Mater. Interfaces 7 (2015) 22807–22813, https://doi.org/10.1021/acsami.5b08665.
[55] M.J. Bovis, S. Noimark, J.H. Woodhams, C.W.M. Kay, J. Weiner, W.J. Peveler, A. Correia, M. Wilson, E. Allan, I.P. Parkin, A.J. MacRobert, Photosensitisation studies of silicone polymer doped with methylene blue and nanogold for antimicrobial applications, RSC Adv. 5 (2015) 54830–54842, https://doi.org/10.1039/C5RA09045H.
[56] M. Katsikogianni, Y.F. Missirlis, Concise review of mechanisms of bacterial adhesion to biomaterials and of techniques used in estimating bacteria-material interactions, Eur. Cell Mater. 8 (2004) 37–57, https://doi.org/10.22203/eCM.v008a05.
[57] Y. Ammar, D.C. Swailes, B.N. Bridgens, J. Chen, Influence of surface roughness on the initial formation of biofilm, Surf. Coat. Tech. 284 (2015) 410–416, https://doi.org/10.1016/j.surfcoat.2015.07.062.